$$r_1\sigma = a_2 - a_1 - S_2(r_2 - r_1) \quad (20)$$

$$\mathbf{r}_{20}\cdot\mathbf{v}_{20} - \mathbf{r}_{10}\cdot\mathbf{v}_{10} = \boldsymbol{\lambda}_0\cdot\mathbf{r}_{10} + \boldsymbol{\epsilon}_0\cdot\mathbf{v}_{20} \quad (21)$$

$$r_{20} - r_{10} = \boldsymbol{\varepsilon}_0\cdot(\mathbf{r}_{10} + \mathbf{r}_{20})/(r_{10} + r_{20}) \quad (22)$$

$$r_2 - r_1 = \boldsymbol{\varepsilon}\cdot(\mathbf{r}_1 + \mathbf{r}_2)/(r_1 + r_2) \quad (23)$$

$$c_2 - c_1 = (a_2 - a_1)/(c_1 + c_2) \quad (24)$$

$$a_2 - a_1 = a_1a_2(b_1 - b_2) \quad (25)$$

$$b_1 - b_2 = 2(r_{20} - r_{10})/r_{10}r_{20} + \boldsymbol{\lambda}_0\cdot(\mathbf{v}_{10} + \mathbf{v}_{20})/\mu \quad (26)$$

In the derivation of Eq. (26) use was made of

$$b = 2/r - v^2/\mu \quad (27)$$

Summary

Given $\mathbf{r}_{10}$, $\mathbf{v}_{10}$, $\boldsymbol{\varepsilon}_0$, $\boldsymbol{\lambda}_0$ at time 0, the steps for finding $\boldsymbol{\varepsilon}$ and $\boldsymbol{\lambda}$ at time t follow: 1) compute $\mathbf{r}_{20} = \mathbf{r}_{10} + \boldsymbol{\varepsilon}_0$, $\mathbf{v}_{20} = \mathbf{v}_{10} + \boldsymbol{\lambda}_0$, $r_{10} = (\mathbf{r}_{10}\cdot\mathbf{r}_{10})^{1/2}$, $v_{10}^2 = \mathbf{v}_{10}\cdot\mathbf{v}_{10}$; 2) compute A_1, B_1, T_1, H_1, D_1, N_1 [equation after (3)], a_1 and b_1 from Eq. (27); 3) solve Kepler's Eq. (1) for C_1; if C_1 is given rather than t, Eq. (1) is used to compute T_1; 4) compute $\mathbf{r}_1$ from Eq. (2) and $r_1 = (\mathbf{r}_1\cdot\mathbf{r}_1)^{1/2}$; 5) compute P_1, S_1, A_2, B_2, H_2, D_2, N_2 [equations after (3)], a_2 and b_2 from Eq. (27); 6) compute in order $\mathbf{r}_{20}\cdot\mathbf{v}_{20} - \mathbf{r}_{10}\cdot\mathbf{v}_{10}$, $r_{20} - r_{10}$, $b_1 - b_2$, $a_2 - a_1$, $c_2 - c_1$ from Eqs. (21, 22, 26, 25, and 24); 7) compute α, β, τ, η, δ, ν from Eqs. (13, 14, 15, 16, 17, 18); 8) compute F, G, T', A', B' from Eqs. (7, 8, 9, 10); 9) solve Eq. (4) for γ; 10) compute Q and R from Eqs. (11) and (12); 11) compute $\boldsymbol{\varepsilon}$ from Eq. (5); 12) compute $\mathbf{r}_2 = \mathbf{r}_1 + \boldsymbol{\epsilon}$, $r_2 = (\mathbf{r}_2\cdot\mathbf{r}_2)^{1/2}$; 13 compute P_2 and S_2 [equations after (3)]; 14) compute ρ and σ from Eqs. (23, 19, 20); 15) compute $\boldsymbol{\lambda}$ from Eq. (6). Since γ will usually be small, $1 - \cos\gamma$ should be replaced by $2\sin^2(\gamma/2)$ for computational purposes.

Numerical Example

We assume the two particles to be in coplanar circular orbits with units chosen such that $a_1^3 = \mu$. The initial conditions are

$$x_{10} = 1,\ y_{10} = 0,\ \dot{x}_{10} = 0,\ \dot{y}_{10} = 1$$

$$\epsilon_{x0} = 0.001,\ \epsilon_{y0} = 0,\ \lambda_{x0} = 0,\ \lambda_{y0} = -0.0004996253122$$

If we let $t = \pi/4$, solve for $\mathbf{r}_1$, $\mathbf{r}_2$, $\mathbf{v}_1$, $\mathbf{v}_2$ at time t and compute $\boldsymbol{\varepsilon}$ and $\boldsymbol{\lambda}$ from the differences $\mathbf{r}_2 - \mathbf{r}_1$ and $\mathbf{v}_2 - \mathbf{v}_1$, we obtain

$$\epsilon_x = 0.0015394491,\ \epsilon_y = -0.0001262154$$

$$\lambda_x = 0.0011853623,\ \lambda_y = 0.0004778069$$

Using the formulas developed in this paper we obtain

$$\epsilon_x = 0.001539449086,\ \epsilon_y = -0.0001262154558$$

$$\lambda_x = 0.001185362260,\ \lambda_y = 0.0004778069038$$

A ten-digit calculator was used for these calculations.

References

[1] Clohessy, W. H. and Wiltshire, R. S., "Terminal Guidance System for Satellite Rendezvous," *Journal of the Aerospace Sciences*, Vol. 27, 1960, pp. 653–658 and 674.

[2] London, H. S., "Second Approximation to the Solution of Rendezvous Equations," *AIAA Journal*, Vol. 1, No. 7, July 1963, pp. 1691–1693.

[3] de Vries, J. P., "Elliptic Elements in Terms of Small Increments of Position and Velocity Components," *AIAA Journal*, Vol. 1, No. 11, Nov. 1963, pp. 2626–2629.

[4] Anthony, M. L. and Sasaki, F. T., "Rendezvous Problem for Nearly Circular Orbits," *AIAA Journal*, Vol. 3, No. 9, Sept. 1965, pp. 1666–1673.

[5] Tschauner, J. and Hempel, P., "Rendezvous zu einem in elliptischer Bahn umlaufenden Ziel," *Astronautica Acta*, Vol. 11, 1965, pp. 104–109.

[6] Euler, E. A. and Shulman, Y., "Second-Order Solution to the Elliptical Rendezvous Problem," *AIAA Journal*, Vol. 5, No. 5, May 1967, pp. 1033–1035.

[7] Battin, R. H., *Astronautical Guidance*, McGraw-Hill, New York, 1964, pp. 46–47.

Fatigue Life Estimation of Fluttering Panels

E. H. Dowell*
Princeton University, Princeton, N.J.

It is now generally appreciated that the development of nonlinear flutter analyses of plates and shells permits the estimation of fatigue life.[1] Such analyses provide not only the dynamic pressure, Mach number, etc., at which flutter begins but also the flutter frequency and stress levels as one penetrates beyond the flutter boundary and into the flutter regime itself. Knowing the stress levels and frequency in the flutter regime, one may use a conventional fatigue curve (stress vs number of cycles to fatigue) to estimate fatigue life for the fluttering panel. It is the purpose of the present Note to provide some examples of fatigue life estimation and discuss their implications for design.

For simplicity, we shall consider an isotropic, rectangular flat plate simply supported on all edges. The principal parameters are (see Ref. 1 for notation)

$$\bar{\sigma}_x = (\sigma_x/E)(a/h)^2\,(1 - \nu^2),\ \text{stress}$$

$$K^2 \equiv \omega^2\rho_m h a^4/D,\ \text{frequency (squared)}$$

$$\lambda^* \equiv 2qa^3/D,\ \text{dynamic pressure}$$

M, Mach number; $\mu = \rho a/\rho_m h$, mass ratio; a/b, length/width. The stress $\bar{\sigma}_x$, and frequency K are determined from the nonlinear flutter analysis when the other parameters, λ^*, M, μ, a/b, are given. Knowing $\bar{\sigma}_x$, K one can determine the dimensional stress, σ_x, and frequency, $f = \omega/2\pi$ for a given panel. From a conventional fatigue curve, given σ_x one may determine the number of cycles to fatigue failure N. The fatigue life is then given by $T = N/f$. For simplicity, we approximate the fatigue curve by an algebraic formula

$$N = (2 \times 10^5/\sigma_x)^6 \quad (1)$$

Equation (1) is a reasonable approximation for aluminum. Furthermore, we shall use the maximum tensile stress in Eq. (1) to determine N. The stress in the panel varies with both position and time. A more complicated rule for determining N could be used where available fatigue data warrant. In particular, the temporal variation of σ_x takes the form of a sinusoidal variation about a mean tensile stress level. In a more precise fatigue life estimate, this mean tensile stress would be taken into account.

In our examples, we shall concentrate on a length/width ratio of two and, for the most part, high supersonic Mach number. Because of the latter, the three parameters λ^*, μ, M may be reduced to two, $\lambda^*/(M^2 - 1)^{1/2}$ and μ/M. In

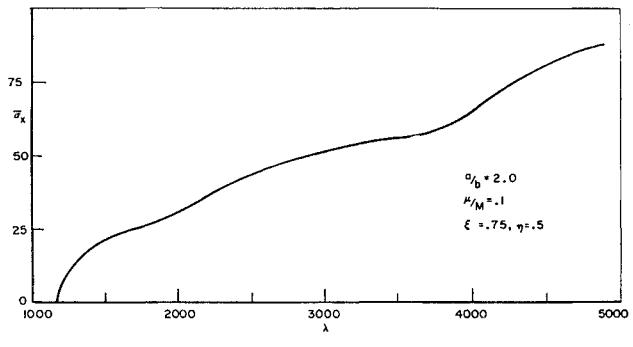

Fig. 1 Stress vs dynamic pressure.

Received April 2, 1970; revision received May 19, 1970. This work was supported by NASA Grant NGR 31-001-146.

* Associate Professor. Member AIAA.

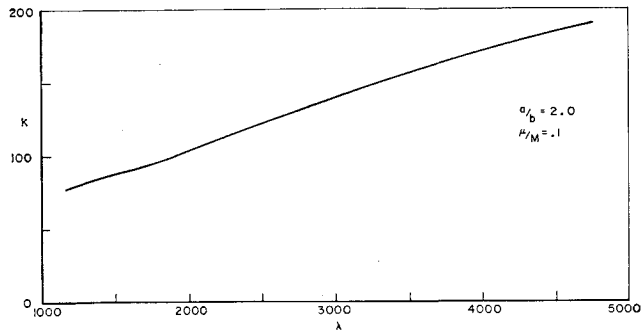

Fig. 2 Frequency vs dynamic pressure.

Figs. 1 and 2, we plot $\bar{\sigma}_x$ and K, respectively, vs λ for $\mu/M = 0.1$ and $a/b = 2$. The results are not very sensitive to variations in μ/M and hence, we fix $\mu/M = 0.1$ in what follows for convenience. Using Figs. 1 and 2, we may look at several design situations. For example, one can fix the material $(\nu E, \rho_m)$ panel dimensions (h,a,b) and examine the variation of fatigue life T vs. dynamic pressure q. In Figs. 3–4, we

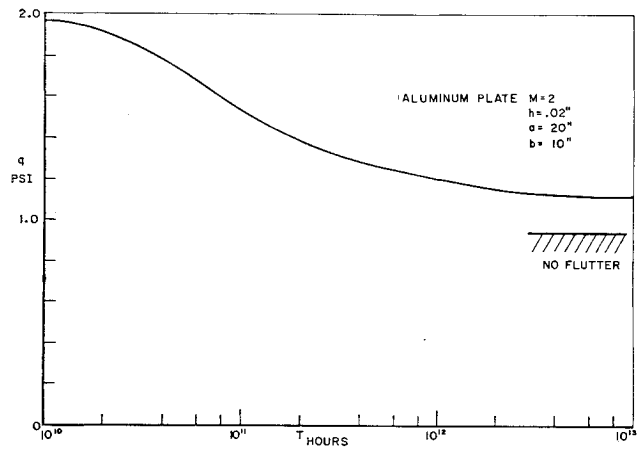

Fig. 3 Dynamic pressure vs fatigue life.

give such results for an aluminum panel of length, $a = 20$ in., width, $b = 10$ in., at $M = 2$ for three thicknesses, $h = 0.02$ in., $h = 0.06$ in., h = 0.2 in. The results for the last case are quite unrealistic, of course, because of the high dynamic pressures. (Recall $q = 41.1$ psi at $M = 2$ at sea level.) However, they help to illustrate a point. Note that for the thinnest panel one may greatly exceed the dynamic

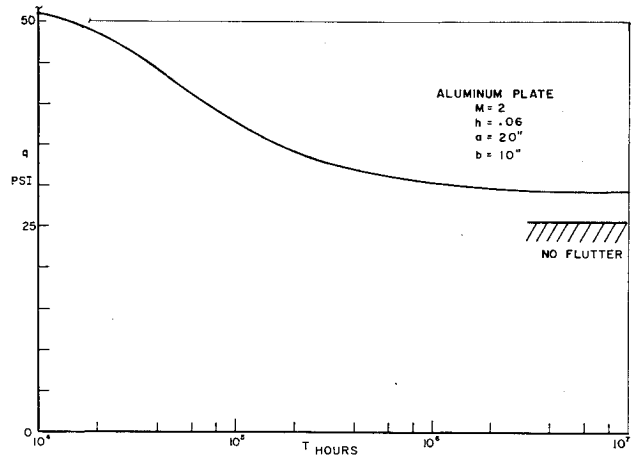

Fig. 4 Dynamic pressure vs fatigue life.

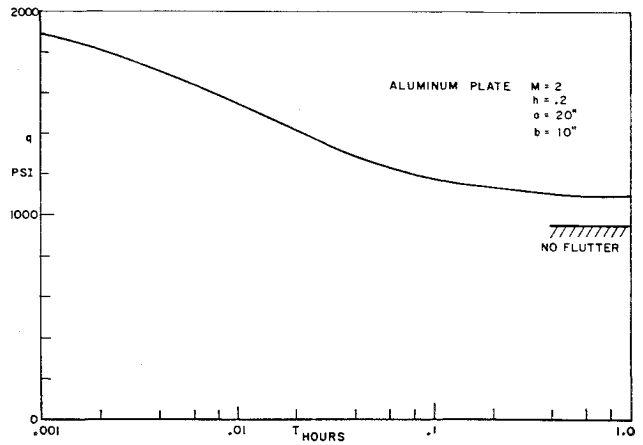

Fig. 5 Dynamic pressure vs fatigue life.

pressure at which flutter begins and still have a long fatigue life. However, for the thickest panel the fatigue life is very short for a small excursion into the flutter regime. Hence, we conclude that whereas a thinner plate will flutter at a lower dynamic pressure than a thicker one, it will be able to exceed its flutter dynamic pressure by a greater amount (on a percentage basis) than a thicker one for a given fatigue life.

Another interesting way of presenting fatigue life data is to consider a given panel (aluminum, a = 20 in., $b = 10$ in., h = 0.06 in.) at a given altitude (sea level) with varying Mach number, see Fig. 6. This panel would begin to flutter at a Mach number of approximately, $M = 0.9$. (For this calculation, the analysis of Ref. 2 was used which employs the full linearized aerodynamic theory valid for lower Mach number.) However, the fatigue life is greater than 5×10^4 hr for $M = 2$. Hence, this panel would have a satisfactory fatigue life for most applications well beyond its flutter Mach number. Finally, we could consider a panel (aluminum, $a = 20$ in., $b = 10$ in.) of varying thickness at a given Mach number and altitude (M = 2, sea level). In Fig. 7, such results are given. As might be expected, fatigue life varies more rapidly with panel thickness than airflow Mach number. However, it appears that significant reductions in panel thickness can be obtained if it is designed for finite rather than infinite (no flutter) fatigue life. What constitutes a reasonable fatigue life varies from flight vehicle to flight vehicle. It ranges from a minute or so (launch vehicle) to tens of thousands of hours (commercial airliner). Of course, in the latter case, only a relatively small portion of the operational life may be flutter critical with a corresponding reduction in design fatigue life.

In conclusion, a capability now exists for fatigue life estimation for panels using nonlinear panel flutter analysis. Based

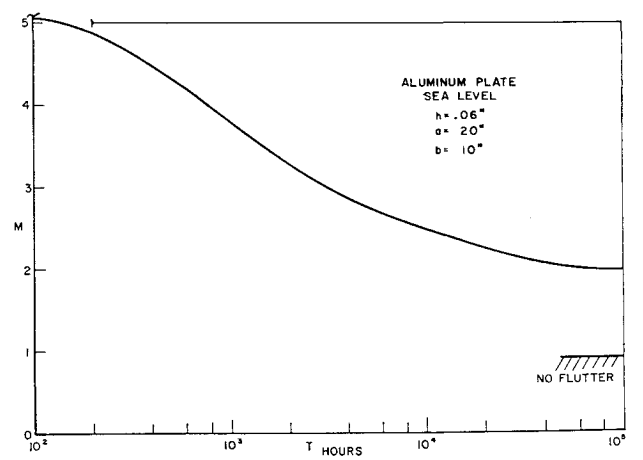

Fig. 6 Mach number vs fatigue life.

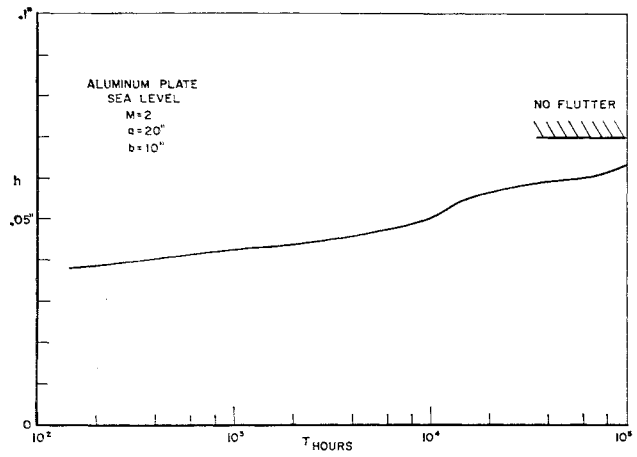

Fig. 7 Plate thickness vs fatigue life.

upon the examples discussed here, significant reductions in panel thickness (or weight) or increases in flight envelope may result from design on the basis of finite fatigue life. This emphasizes the need for an experimental investigation to assess the accuracy of available theory in predicting flutter stress levels and fatigue life.

References

[1] Dowell, E. H., "Panel Flutter: A Review of the Aeroelastic Stability of Plates and Shells," *AIAA Journal*, Vol. 8, No. 3, March 1970, pp. 385–399.

[2] Dowell, E. H., "Nonlinear Oscillations of a Fluttering Plate—II," *AIAA Journal*, Vol. 5, No. 10, Oct. 1967, pp. 1856–1862.

Experimental Evaluation of a Subsonic Ludwieg Tube

PHILIP C. MALTE* AND KENNETH R. SIVIER†
The University of Michigan, Ann Arbor Mich.

A SUBSONIC Ludwieg[1] tube, or simple expansion tube, can supplement a shock tube as an aerodynamic testing facility. For example, the convective flow behind the centered expansion wave propagating in the tube can be used to accelerate small solid particles and thereby measure drag forces pertinent to two-phase flow systems. In the subsonic mode, the Ludwieg tube has five times the useful flow duration of an equivalent length shock tube.[2] Furthermore, a Ludwieg tube may complement a shock tube in studies concerning the effect of flow expansion on chemical reaction rates. However, before being used as an investigative device, the flow characteristics of the tube must be determined; the results presented herein summarize experiments conducted for this purpose and reported in Ref. 2.

The Ludwieg tube tested consisted of a pipe 15 ft in length with a 3.1-in. i.d. The centered expansion wave was initiated at a diaphragm located between the pipe and a dump tank. Upon diaphragm rupture, the unsteady expansion wave, assumed centered at the rupture point, propagated upstream into the quiescent high-pressure air contained within the pipe; the shock wave created at rupture spread into the dump tank and rapidly weakened. The shock wave was assumed of insignificant importance; the main change in the pressure level of the dump tank was caused by the mass addition. Furthermore, no reflected shock was ever observed in the pipe. The subsonic Ludwieg tube with corresponding wave diagram is shown in Fig. 1. Pressure transducers and an impact tube were used to monitor static and total pressure 9 in. from the rupture point. Also, for comparison the static pressure was measured 3 ft from the rupture point. For flow Mach numbers below 0.7 the expansion wave was thin; the durations of the useful expanded flow were, respectively, 20 msec and 15 msec at the 9-in. and 3-ft observations points. The expansion wave approached "infinite" time duration for sonic conditions. All durations agreed closely with the isentropic unsteady theory of Ref. 3. Furthermore, the expansion wave as observed was always well formed, as indicated by typical pressure traces shown in Fig. 2.

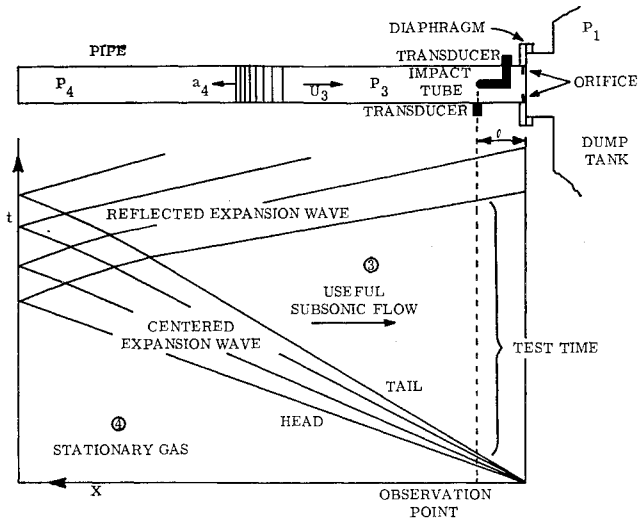

Fig. 1 Subsonic Ludwieg tube.

The steadiness of the convective flow behind the expansion wave was examined in some detail. While several authors, principally Mirels,[4,5] have shown the effect of boundary layers on flow in shock tubes, we encountered few investigations concerning the flow behing an isolated unsteady expansion wave. In our investigation, the induced flow was quasi-steady, the second-order variations being caused by the action of the boundary layer and by the rising dump tank pressure. The effect of the boundary layer was further expansion; with increased distance behind the expansion wave (or increased time at a fixed observation point) the pressure decreased and the Mach number inferred from pressure measurements increased. The rising tank pressure induced weak compression waves that propagated upstream, thereby caus-

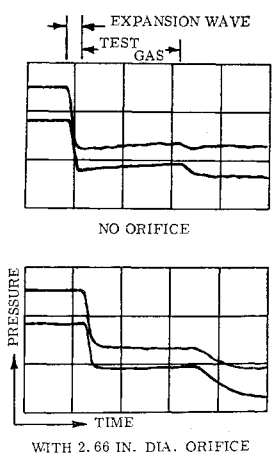

Fig. 2 Oscilloscope pressure traces: static pressure, top; impact pressure, bottom. 0.2 psi/div, 10 msec/div. l = 9 in., $M_3 \cong 0.4$, $Re \cong 1.8 \times 10^4$.

Received April 20, 1970; revision received May 18, 1970. This work was supported by NASA Grant N]G 86-60.

* Graduate Student, Department of Aerospace Engineering; currently on leave-of-absence from Martin Marietta Corp., Denver, Colo. Student Member AIAA.

† Associate Professor, Aeronautical and Astronautical Engineering Department, University of Illinois, Urbana, Ill. Member AIAA.